ZnO Microflowers Grown by Chemical Bath Deposition: A Low-Cost Approach for Massive Production of Functional Nanostructures

Vincenzina Strano [1],* [ID]**, Maria Grazia Greco [2], Enrico Ciliberto [2] and Salvo Mirabella [1],***

[1]   CNR-IMM Matis and Dipartimento di Fisica e Astronomia Università di Catania, via S. Sofia 64, 95123 Catania, Italy

[2]   Dipartimento di Scienze Chimiche Università di Catania, via S. Sofia 64, 95123 Catania, Italy; mgrazia.uni@gmail.com (M.G.G.); cilibert@unict.it (E.C.)

*   Correspondence: vincenzina.strano@ct.infn.it (V.S.); salvatore.mirabella@ct.infn.it (S.M.)

check for updates

Abstract: The massive production of nanostructures with controlled features and high surface area is a challenging and timely task in view of developing effective materials for sensing and catalysis. Herein, functional ZnO nanostructures, named microflowers (MFs) have been prepared by a facile and rapid chemical bath deposition. ZnO MFs show an intriguing sheets-composed spheroidal shape, with diameters in the range 0.2–2.5 μm, whose formation is achieved by a complexing action by F in an aqueous solution of zinc nitrate hexahydrate and hexamethylenetetramine. The evolution of the physical and structural properties of the material, following post-deposition thermal annealing, has been investigated by scanning electron microscopy (SEM), energy dispersive X-ray analyses (EDX), photoluminescence (PL) and X-ray diffraction (XRD) techniques. The effectiveness of ZnO MFs in UV detection has also been tested to account for the potentiality of these nanostructures.

Keywords: ZnO; chemical bath deposition; nanostructures; massive production; UV detection

1. Introduction

The synthesis of advanced materials via aqueous solution represents a solid route for the fabrication of high-quality thin films and nanostructures [1,2]. Such techniques allow a number of advantages such as a low-temperature process, simple laboratory setup, relatively high growth rate and costs containment [1,2]. Among all, the chemical bath deposition (CBD) is one of the most used and studied methods for the synthesis, in particular, of functional metal chalcogenides and oxides [1,3–5]. In CBD, the nucleation and growth of the material typically take place within a precursor solution, allowing a great versatility: the particular composition of the chemical bath strongly affects the morphology of the material as well as the solution pH, temperature, reagent concentrations and duration of the synthesis. All of these parameters, easily controllable, have effects on the shape and the physico-chemical properties of the grown structures [6–11]. A shining example of the development of CBD is the wide variety of zinc oxide (ZnO) nanostructures achievable via this method, spanning from nanorods to nanowalls, from nanotubes to nanoplates [8,10,12–15]. In the last 20 years, a remarkable interest has been generated by ZnO nanostructures [16,17] because of the unique combination of material properties and nanotechnology, enabling a variety of applications, as in sensors and in electro-optical devices [17–22].

ZnO is biocompatible and abundant in nature and its production through CBD is sustainable from the economic and environmental points of view [17,23,24]. The CBD of ZnO nanostructures on substrates ensures high rate and uniformity over the whole area of the samples [10,12,25]. Among the many advantages, the use of a substrate allows the creation of arrays of ordered and aligned

nanostructures, as in the case of ZnO nanorods, as well as the easy selective deposition, as in the case of ZnO nanowalls growing only on aluminum-covered areas [8,11,21]. The CBD allows also the substrate-free synthesis of ZnO nanopowders, consisting of nanostructures homogeneously nucleated in solution, highly promising for scaling up and for all applications requiring a massive fabrication of nanostructures [26–28].

In the present work, CBD is developed to obtain ZnO microflowers (MFs), an open-structure with extended and highly reactive surface area. The ZnO MFs are composed of very thin sheets organized to form a spherical structure characterized by a large surface-to-volume ratio, representing a key-factor in sensing mechanisms. In particular, ZnO MFs have been demonstrated to be a key element in the fast detection of UV light.

2. Materials and Methods

Starting from the well-known chemical system based on an aqueous solution of zinc nitrate and hexamethylenetetramine (HMTA) [10], the production of ZnO microflowers is attained by CBD, adding ammonium fluoride to the bath. This specific approach is presented here for the first time (to the best of our knowledge). A total of 50 mL solutions of zinc nitrate hexahydrate ($Zn (NO_3)_2 \times 6 H_2O$, purum p.a., crystallized, ≥99%, Sigma-Aldrich, Italy) 25 mM, HMTA, ($(CH_2)_6N_4$, puriss. p.a., Reag. Ph.Eur., ≥99.5%, Sigma Aldrich, Italy) 25 mM and ammonium fluoride (NH_4F, ≥99.99%, Sigma-Aldrich, Italy) 16 mM, were placed in thermostatically-controlled bath at 90 °C. Each solution was prepared separately with deionized water (MilliQ, 18 MΩ cm). Once the thermal equilibrium is reached in each one, the three solutions were mixed in a large beaker, and, after five minutes, a white-color precipitate occurred, containing the ZnO MFs. It is worth reporting that several experimental attempts have shown that the mixing of the three reagents as heated solution represents a key step for ensuring a uniform synthesis of MFs. Other procedures, as the mix of all the reagents before heating or the late addition of NH_4F, have given rise to the formation of variegated nanostructures. Figure 1a summarizes the one-pot synthesis of ZnO MFs. The growth solution was then transferred to Eppendorf tubes, the precipitate was separated by centrifugation (10 min, 9000 rpm) and washed four times with deionized water. A part of the obtained product was deposited by spin coating (60 s, 1000 rpm), on a silicon substrate for the characterization of the as-grown material. The powder of MFs was then annealed at 350 °C for 1 h in N_2.
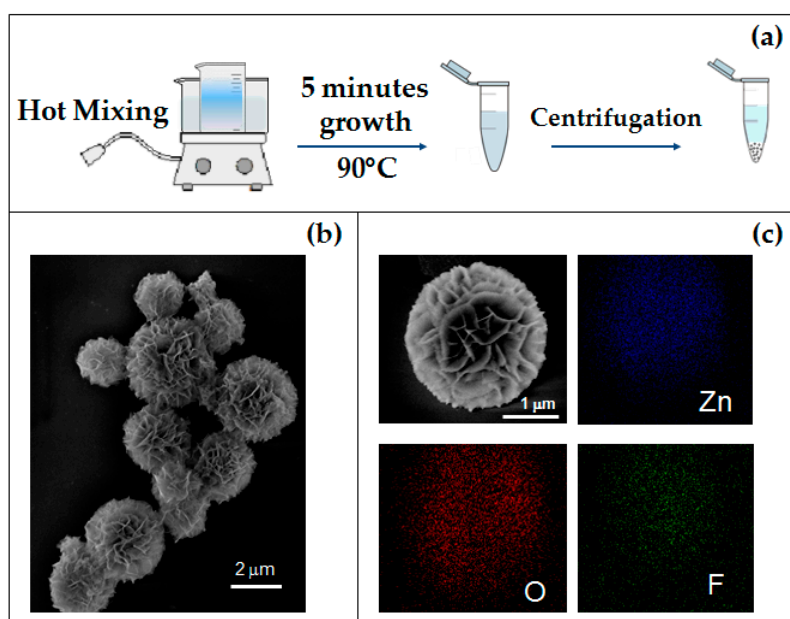

Figure 1. (**a**) Schematic synthesis diagram of the 3D flower-like hierarchical ZnO microstructures; (**b**) SEM image of as-grown MFs; (**c**) SEM image of a single MF and corresponding EDX elemental maps.

The material was characterized by different techniques, including scanning electron microscopy (SEM, Gemini field emission SUPRA 25 Carl Zeiss, Germany) equipped with energy-dispersive X-Ray spectrometer (EDX), X-Ray diffraction (XRD, AXDS D5005 Bruker Italy, Cu Kα radiation, λ = 1.542 Å) and photoluminescence spectroscopy (PL) using He-Cd laser (λ = 325nm) as excitation source. Room temperature electrical measurements were conducted on annealed ZnO MFs deposited by spin coating (60 s,1000 rpm) on Au interdigitated electrodes (IDE) with three fingers for each electrode (200 μm long, spaced 20 μm each other), realized on a glass substrate by using a conventional photolithography method.

3. Results and Discussion

Figure 1b shows the SEM image of the as-grown MFs. It can be noted that these spheroidal structures, with diameters ranging from 200 nm to 2.5 μm, are actually composed of auto-assembled nanosheets with a common nucleus. In order to investigate the chemical composition of the structures, MFs placed on an Si substrate were characterized by EDX analysis. Figure 1c shows the SEM image of a single as-grown MF and its corresponding EDX elemental-maps. The results confirmed the obvious presence of zinc and oxygen, evidencing also some fluorine traces. The SEM micrograph of MFs annealed at 350 °C is reported in Figure 2a. Comparing the morphology of as-grown and annealed MFs (Figures 1b and 2a, respectively), it seems that the shape of the structures does not undergo any variation. On the other hand, the elemental composition after thermal treatment is slightly different. The EDX spectra shown in Figure 2b reveal that the traces of fluorine disappear after the annealing at 350 °C for 1 h. Structural variations are confirmed by XRD analysis: Figure 2c shows XRD patterns of as-grown and annealed samples and, as expected [29,30], the crystal quality significantly improves after the thermal treatment, revealing the typical hexagonal ZnO structure.
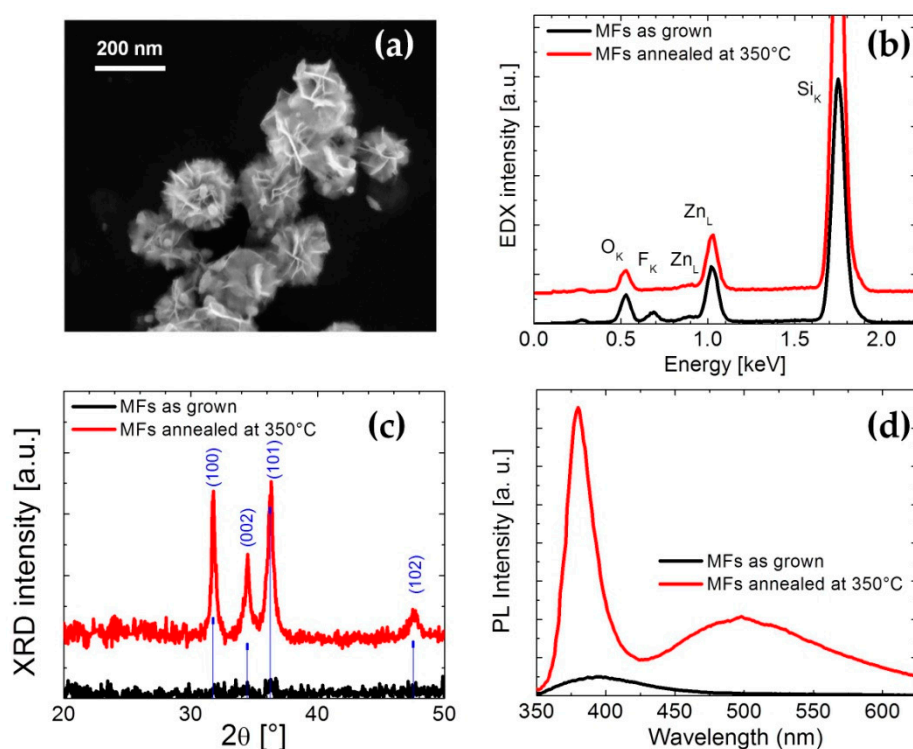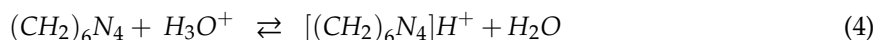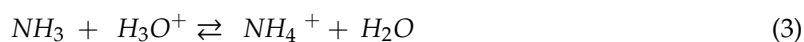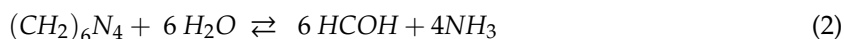

Figure 2. (**a**) SEM image of MFs after annealing treatment at 350 °C in air for 20 min, (**b**) EDX analyses of as grown and annealed MFs, (**c**) XRD patterns of as grown and annealed MFs and (**d**) PL spectra of the same samples.

The effect of annealing on the room temperature photoluminescence spectra is shown in Figure 2d. The PL spectrum of annealed MFs exhibits a peak centered at 386 nm, attributed to the near band edge-emission from the recombination of free excitons [31,32], and a broad band in the visible region (450–700 nm), coming from the radiative recombination involving defect states [9]. The room temperature-PL spectrum of the as-grown ZnO MFs shows only a weak and broad emission band at around 400 nm.

The experimental results suggested that the as-grown MFs, coming from a quasi-immediate homogeneous nucleation in solution, consist of zinc compounds that are totally transformed in ZnO only after the annealing process. Studies on growth kinetics (not shown), conducted by taking samples from the solution at different times (30, 60, 120, 180, 300 s), have shown that the size of the diameter of MFs is not a linear function of the growth time evidencing a non-uniform nucleation in the bulk solution. In aqueous solution the zinc salt dissociates and the Zn^{2+} ions form a complex with six water molecules $[Zn(H_2O)_6]^{2+}$ [10]:

$$[Zn(H_2O)_6]^{2+} + H_2O \rightleftarrows [Zn(H_2O)_5OH]^+ + H_3O^+ \tag{1}$$
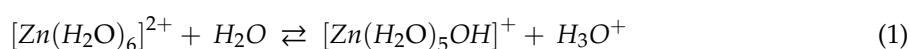
On the other hand, the hexamethylenetetramine (HMTA) molecules undergo decomposition or protonation processes:

$$(CH_2)_6N_4 + 6\,H_2O \rightleftarrows 6\,HCOH + 4NH_3 \tag{2}$$

$$NH_3 + H_3O^+ \rightleftarrows NH_4^+ + H_2O \tag{3}$$

$$(CH_2)_6N_4 + H_3O^+ \rightleftarrows [(CH_2)_6N_4]H^+ + H_2O \tag{4}$$

In a heated aqueous bath containing both $Zn(NO_3)_2$ and HMTA, the latter and the as-formed NH_3 act as ligands coordinating the Zn^{2+} ions and control the concentration of free zinc ions present in solution [10]. Therefore, under chemical bath deposition conditions, zinc nitrate and HMTA typically produce high-quality nanorods of ZnO since the equilibria established in solution promotes an anisotropic growth along the (0001) direction (for nanorods nucleated both homogeneously in solution and heterogeneously on a substrate) [5,10,12]. Variation of the precursor composition and the addition of effective complexing agents enable the synthesis of different morphology [14,15,33]. NH_4F also dissolved in water:

$$NH_4F + H_3O^+ \rightarrow NH_4^+ + F^- \tag{5}$$

$$NH_4^+ + H_2O \rightarrow NH_3 + H_2O \tag{6}$$
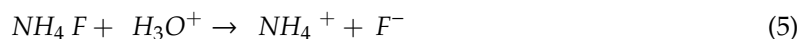
Simple considerations lead to affirm that the formation of micro-flowers takes place in a slightly acidic environment. As reported in ref. 10, the aqueous solution containing only zinc nitrate is acidic (pH =4.2) while the presence of HMTA, due to its strong pH regulation activity, stabilized the pH value around at 5.7. Such value is reasonably little changed by the addition of NH_4F solution. The formation of the microflower structure may be associated to mechanisms similar to those extensively reported in the literature for other two-dimensional zinc-based nanostructure, resulting strongly dependent on the solution chemistry [4,30,34,35]. The layered basic zinc salts (LBZS), for example, are species characterized by a lamellar structure, with high surface area, that, under particular conditions of synthesis [36], represent an intermediate phase of the formation of ZnO in solution. A particular ZnO sheets-like nanostructure is represented by nanowalls [8,30,37,38] that is commonly generated in a zinc salt-based aqueous solution using an Al-covered substrate. It was observed that the Al has a significant role in generating the morphological shape of the nanowalls through the $Al(OH)_4^-$ species, forming in solution. $Al(OH)_4^-$ promote the lateral growth of Zn-based nanostructure by binding the Zn^{2+} terminated planes and obstructing the growth along the (0001) direction. This is also confirmed by the fact that the growth rate and the quality of ZnO NWLs are affected by the generation rate of $Al(OH)_4^-$ [8,37,38]. Post-annealing processes were demonstrated to convert the as-grown nanowalls in pure ZnO [30]. In our case, the bath composition and the duration of the synthesis lead to the formation

of microflowers, amorphous layered structures, as revealed by the structural and morphological analyses (Figure 2). It is reasonable to assume that the presence of ammonium fluoride favors the formation of the microflower-structure in the same way as the aluminium promotes the creation of the nanowall-structure. Wang et al. [33] have studied the conditions for varying the morphology of ZnO nanostructures grown by chemical precipitation, by tuning the Zn^{2+}: OH^- ratio in the precursor solution and modifying the amount of NH_4F used as complexing agent and pH adjuster. Moreover, many authors reported the use of NH_4F for the formation of $Zn(OH)F$ [36,39]. In particular, Yamabi et al. [38] have conducted a comprehensive study on the growth of wurtzite film of ZnO in aqueous solution. They have investigated the effect of different ammonium salts (NH_4F, NH_4Cl, NH_4NO_3 and $(NH_4)_2SO_4$) as complexing agents in the growth of wurtzite zinc oxide, observing a stronger coordination of F^- to Zn^{2+} than in the case of the other counter anions. They reported that an acidic pH condition of the solution favors the precipitation of zinc hydroxides considered a metastable phase. On the other hand, at pH <7.8 Zn^{2+} ions can coordinate with F^- anions, affecting the growth processes in solution. It may be the case of our study in which the fluoride ions F^-, attaches to the Zn^{2+} terminated planes of the growing structure, as revealed by the traces of fluoride in the as-grown MFs in EDX analysis (Figure 2b), validating the role of fluoride as complexing agent in engendering the nanosheets. During thermal annealing, F leaves the MFs most probably forming volatile HF by using protons of OH species.

The CBD of MFs offers a number of advantages. The synthesis is substrate-free, low cost and fast. Furthermore, we calculated a material yield of at least 10 g of MFs powder per liter of solution, confirming the great potential of such approach for high-volume productions. The MFs, by virtue of their morphology, offer a very large exposed surface area, turning out to be structurally ideal for a number of applications especially those whose performances are greatly increased by high surface-to-volume ratios, as in sensors. As described in the literature, the photo-detection mechanism in ZnO structures is essentially based on the absorption–desorption of atmospheric oxygen occurring at the surface that causes a change in the conductivity of ZnO. The width of ZnO exposed area and the nature of the native defects in ZnO (as zinc and oxygen vacancies) were proven to have an important role in defining the UV-sensing performance [9,16,40].

As a proof of concept, the ability of ZnO MFs in detecting UV light was analyzed by simply dispersing the annealed MFs on gold microelectrodes and collecting their electrical response under UV illumination. The Figure 3a,b reporting the SEM micrograph in tilted view of MFs spun on Au IDE, reveal that MFs agglomerates actually act as bridge for the Au fingers in several region of IDE. Indeed, the current-voltage characteristic of ZnO MFs, between −1 V and 1 V, showed a ohmic behavior (not shown). In order to investigate the electrical response of the sample under UV exposure, measurements of the current over time were carried out, applying a constant bias voltage of 1 V. The sample was illuminated by a 250 W tungsten halogen lamp containing a UV component (albeit weak) while a long-pass yellow filter was used for blocking radiation with wavelength lower than 500 nm. In Figure 3c, the current output is reported: at the beginning, the sample was in dark condition and a stable current of 1.05 ± 0.03 nA is detected. After 80 s, the lamp was turned on and the current started to exponentially increase followed by an exponential decrease when the light is turned off, at the time of 220 s. In order to exclude a possible contribution to the increase of the photocurrent due to the absorption of the green part of the lamp spectrum, the sample was illuminated by the halogen lamp filtered by the long-pass yellow filter and no current variation was detected with respect to the dark condition. The response ($\tau_{response}$) and reset ($\tau_{recovery}$) times of the system were extracted from the exponential fit of the photocurrent rise and decay curves:

$$\tau_{response} = 47 \text{ s} \pm 0.5 \text{ s}$$

$$\tau_{recovery} = 51 \text{ s} \pm 0.5 \text{ s}$$

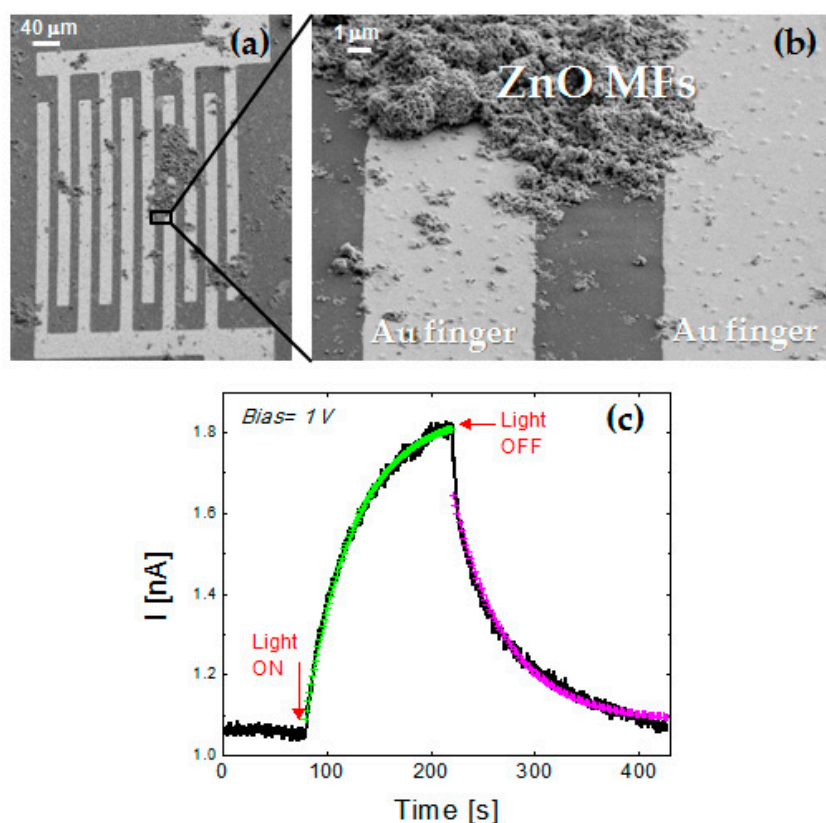**Figure 3.** (**a**,**b**) SEM micrograph in tilted view of annealed MFs on a gold IDE at different magnification. (**c**) Photocurrent response to the light exposure (halogen lamp with UV component) under a bias voltage of 1 V.

The above results are in agreement with the value ranges reported in the literature [40–43]. The slow response to UV illumination is partially determined by the desorption kinetics of the atmospheric oxygen molecules induced by UV photons [40,41]. At ambient conditions, oxygen molecules were absorbed in correspondence with oxygen vacancies at ZnO surface. Under UV light, electron–hole pairs are created, the holes migrate to the surface causing the oxygen desorption while the unpaired electrons are collected to the anode with an increase of the photocurrent. When the UV illumination is turned off, the initial condition is restored with a gradual current decay [44]. The wide surface area offered by the MFs is a fundamental advantage, being the UV detection a surface mechanism. Further tests will be needed in order to deeply investigate the response of the ZnO MFs to UV exposure and to identify the factors affecting the sensing performance (concentration of initial MFs dispersion, geometry of IDE, detection area, ohmic contacts and so on).

4. Conclusions

In summary, a high-yield, low-cost, fast and easy chemical bath synthesis of Zn-based microflowers, spheroidal mesoporous structures with high surface-to-volume ratio, is reported. The formation of the particular layered structure of the MFs is ascribed to the complexing action of fluoride. Morphological and structural analyses showed that the amorphous as-grown nanostructures are transformed in pure ZnO, maintaining the same shape. The UV response of ZnO MFs was tested and the results clearly confirm that ZnO MFs are promising low-cost nanostructures for the construction of UV sensors.

Author Contributions: Conceptualization, S.M. and E.C.; investigation: (1) ZnO MFs synthesis, M.G.G., (2) SEM and EDX analyses, V.S., M.G.G., S.M. (3) electrical characterization, V.S., M.G.G., (4) PL characterization, S.M., (5) XRD analyses, V.S., M.G.G.; methodology: S.M., V.S., M.G.G.; formal analysis: V.S., S.M.; writing—original draft preparation, V.S., M.G.G., S.M.; writing—review and editing, S.M., V.S., M.G.G., E.C.

References

1. Schneller, T.; Waser, R.; Kosec, M.; Payne, D. *Chemical Solution Deposition of Functional Oxide Thin Films*, 1st ed.; Springer: Heidelberg, Germany; New York, NY, USA; Dordrecht, The Netherlands; London, UK, 2013; pp. 1–796.

2. Hodes, G. Semiconductor and ceramic nanoparticle films deposited by chemical bath deposition. *Phys. Chem. Chem. Phys.* **2007**, *9*, 2181–2196. [CrossRef]

3. Li, G.; Wang, X.; Liu, L.; Liu, R.; Shen, F.; Zheng, C.; Chen, W.; Zhang, T. Controllable synthesis of 3D $Ni(OH)_2$ and NiO nanowalls on various substrates for high-performance nanosensors. *Small* **2015**, *6*, 731–739. [CrossRef]

4. Hosono, E.; Fujihara, S.; Kimura, T. Fabrication and electrical properties of micro/nanoporous ZnO:Al films. *J. Mater. Chem.* **2004**, *14*, 881–886. [CrossRef]

5. Vayssieres, L.; Keis, K.; Lindquist, S.-E.; Hagfeldt, A. Purpose-built anisotropic metal oxide material: Highly oriented microrod array of ZnO. *J. Phys. Chem. B* **2001**, *105*, 17–3350. [CrossRef]

6. Govender, K.; Boyle, D.S.; Kenway, P.B.; O'Brien, P. Understanding the factors that govern the deposition and morphology of thin films of ZnO from aqueous solution. *J. Mater. Chem.* **2004**, *14*, 2575–2591. [CrossRef]

7. Guillemin, S.; Rapenne, L.; Roussel, H.; Sarigiannidou, E.; Bremond, G.; Consonni, V. Formation Mechanism of ZnO Nanowires: The crucial role of crystal orientation and polarity. *J. Phys. Chem. C* **2013**, *117*, 20738–20745. [CrossRef]

8. Iwu, K.O.; Strano, V.; Di Mauro, A.; Impellizzeri, G.; Mirabella, S. Enhanced quality, growth kinetics and photocatalysis of ZnO nanowalls prepared by chemical bath deposition. *Cryst. Growth Des.* **2015**, *15*, 4206–4212. [CrossRef]

9. Barbagiovanni, E.G.; Reitano, R.; Franzò, G.; Strano, V.; Terrasi, A.; Mirabella, S. Radiative mechanism and surface modification of four visible deep level defect states in ZnO nanorods. *Nanoscale* **2016**, *8*, 995–1006. [CrossRef]

10. Strano, V.; Urso, R.G.; Scuderi, M.; Iwu, K.O.; Simone, F.; Ciliberto, E.; Spinella, C.; Mirabella, S. Double role of HMTA in ZnO nanorods grown by chemical bath deposition. *J. Phys. Chem. C* **2014**, *118*, 28189–28195. [CrossRef]

11. Pellegrino, D.; Franzò, G.; Strano, V.; Mirabella, S.; Bruno, E. Improved synthesis of ZnO nanowalls: Effect of chemical bath deposition time and annealing temperature. *Chemosensors* **2019**, *7*, 18. [CrossRef]

12. Greene, L.E.; Law, M.; Goldberger, J.; Kim, F.; Johnson, J.C.; Zhang, Y.; Sayakally, R.J.; Yang, P. Low-temperature wafer-scale production of ZnO nanowire arrays. *Angew. Chem. Int. Ed.* **2003**, *42*, 3031–3034. [CrossRef]

13. Ahsanulhaq, Q.; Kim, S.H.; Kim, J.H.; Hahn, Y.B. Structural properties and growth mechanism of flower-like ZnO structures obtained by simple solution method. *Mater. Res. Bull.* **2008**, *23*, 3483–3489. [CrossRef]

14. Bingqiang, C.; Weiping, C. From ZnO Nanorods to Nanoplates: Chemical bath deposition growth and surface-related emissions. *J. Phys. Chem. C* **2008**, *112*, 680–685.

15. Manthina, V.; Agrios, A.G. Single-pot ZnO nanostructure synthesis by chemical bath deposition and their applications. *Nano-Struct. Nano-Objects* **2016**, *7*, 1–11. [CrossRef]

16. Janotti, A.; Van de Walle, C.G. Fundamentals of ZnO as semiconductor. *Rep. Prog. Phys.* **2009**, *72*, 126501. [CrossRef]

17. Kołodziejczak-Radzimska, A.; Jesionowski, T. Zinc oxide-from synthesis to application: A review. *Materials* **2014**, *7*, 2833. [CrossRef]

18. Wang, Z.L.; Song, J. Piezoelectric nanogenerators based on zinc oxide nanowire arrays. *Science* **2006**, *312*, 242–246. [CrossRef]

19. Sang, L.; Liao, M.; Sumiya, M. A comprehensive review of semiconductor ultraviolet photodetectors: From thin film to one-dimensional nanostructures. *Sensors* **2013**, *13*, 10482–10518. [CrossRef]

20. Al-Hilli, S.; Willander, M. The pH Response and Sensing Mechanism of n-Type ZnO/Electrolyte Interfaces. *Sensors* **2009**, *9*, 7445–7480. [CrossRef]

21. Maiolo, L.; Mirabella, S.; Maita, F.; Alberti, A.; Minotti, A.; Strano, V.; Pecora, A.; Schacam-Diamand, Y.; Frotunato, G. Flexible pH sensors based on polysilicon thin film transistors and ZnO nanowalls. *Appl. Phys. Lett.* **2014**, *105*, 093501. [CrossRef]

22. Bruno, E.; Strano, V.; Mirabella, S.; Donato, N.; Leonardi, S.G.; Neri, G. Comparison of ZnO nanowalls-based sensors toward low concentration on CO and NO₂. *Chemosensors* **2017**, *5*, 20. [CrossRef]

23. Gopikrishnan, R.; Zhang, K.; Ravichandran, P.; Baluchamy, S.; Ramesh, V.; Biradar, S.; Ramesh, P.; Pradhan, J.; Hall, J.C.; Pradhan, A.K.; et al. Synthesis, characterization and biocompatibility studies of zinc oxide (ZnO) nanorods for biomedical application. *Nano-Micro Lett.* **2010**, *2*, 31–36. [CrossRef]

24. Zhang, Y.; Nayak, T.R.; Hong, H.; Cai, W. Biomedical applications of zinc oxide nanomaterials. *Curr. Mol. Med.* **2013**, *13*, 1633–1645. [CrossRef] [PubMed]

25. Cheng, J.P.; Zhang, X.B.; Luo, Z.Q. Oriented growth of ZnO nanostructures on Si and Al substrates. *Surf. Coat. Technol.* **2008**, *202*, 4681–4686. [CrossRef]

26. Amin, G.; Sandberg, M.O.; Zainelabdin, A.; Zaman, S.; Nur, O.; Willander, M. Scale-up synthesis of ZnO nanorods for printing inexpensive ZnO/polymer white light-emitting diode. *J. Mater. Sci.* **2012**, *47*, 4726–4731. [CrossRef]

27. Shim, J.W.; Kim, J.W.; Han, S.H.; Chang, I.S.; Kim, H.K.; Kang, H.H.; Lee, O.S.; Suh, K.D. Zninc oxide/polymethylmetacrylate composite microspheres by in situ suspension polymerization and their monphological study. *Colloids Surf. A* **2002**, *207*, 105–111. [CrossRef]

28. Tian, C.; Zhang, Q.; Wu, A.; Jiang, M.; Liang, Z.; Jiang, B.; Fu, H. Cost-effective large scale synthesis of ZnO photocatalyst with excellent performance for dye photodegradation. *Chem. Commun.* **2012**, *48*, 2858–2860. [CrossRef]

29. Mathew, J.P.; Varghese, G.; Mathew, J. Effect of post-thermal annealing on the structural and optical properties of ZnO thin films prepared from polymer precursor. *Chin. Phys. B* **2012**, *21*, 078104. [CrossRef]

30. Scuderi, M.; Strano, V.; Spinella, C.; Nicotra, G.; Mirabella, S. Low-cost synthesis of pure nanowalls showing three-fold symmetry. *Nanotechnology* **2018**, *29*, 135707. [CrossRef]

31. Wang, L.; Giles, N.C. Temperature dependence of the free-exciton transition energy in zinc oxide by photoluminescence excitation spectroscopy. *J. Appl. Phys.* **2003**, *94*, 973. [CrossRef]

32. Tang, Z.K.; Kawasaki, M.; Ohtomo, A.; Koinuma, H.; Segawa, Y. Self-assembled ZnO nano-crystal and exciton lasing at room temperature. *J. Cryst. Growth* **2006**, *287*, 169–179. [CrossRef]

33. Yamabi, S.; Imai, H. Growth conditions for wurtzite zinc oxide films in aqueous solutions. *J. Mater. Chem.* **2002**, *12*, 3773–3778. [CrossRef]

34. Wang, M.; Zhang, Y.; Zhou, Y.; Yang, F.; Kim, E.J.; Hahn, S.H.; Seong, S.G. Rapid room-temperature synthesis of nanosheet.assembled ZnO mesocrystals with excellent photocatalytic activity. *CrystEngComm* **2013**, *15*, 754–763. [CrossRef]

35. Song, B.; Cui, X.; Wang, Y.; Si, L.; Kou, Z.; Tian, W.; Yi, C.; Sun, Y. Controllable growth of unique three-dimensional layered basic zinc salt/ZnO binary structure. *Cryst. Growth Des.* **2016**, *16*, 4877–4885. [CrossRef]

36. Huang, Q.L.; Wang, M.; Zhong, H.X.; Chen, X.T.; Xue, Z.L.; You, X.Z. Netlike nanostructures of Zn(OH)F and ZnO: Synthesis, characterization and properties. *Cryst. Growth Des.* **2008**, *8*, 1412–1417. [CrossRef]

37. Feng, Y.; Wang, G.; Liao, J.; Chen, C.; Li, M.; Li, Z. Honeycomb-like ZnO mesoporous nanowall arrays modified with Ag nanoparticles for highly efficient photocatalytic activity. *Sci. Rep.* **2017**, *7*, 11622. [CrossRef]

38. Yu, L.; Wei, J.; Luo, Y.; Tao, Y.; Lei, M.; Fan, X.; Yan, W.; Peng, P. Dependence of Al3+ on the growth mechanism of vertical standing ZnO nanowalls and their NO2 gas sensing properties. *Sens. Actuators B* **2014**, *204*, 96–101. [CrossRef]

39. Saito, N.; Haneda, H.; Seo, W.S.; Koumoto, K. Selective deposition of ZnF(OH) on self-assembled monolayers in Zn-NH4F aqueous solutions for micropatterning of zinc oxide. *Langmuir* **2001**, *17*, 1461–1469. [CrossRef]

40. Barbagiovanni, E.G.; Strano, V.; Franzò, G.; Crupi, I.; Mirabella, S. Photoluminescence transient study of surface defects in ZnO nanorods grown by chemical bath deposition. *Appl. Phys. Lett.* **2015**, *106*, 093108. [CrossRef]

41. Gupta, S.P.; Pawbake, A.S.; Sathe, B.R.; Late, D.J.; Walke, P.S. Superior humidity sensor and photodetector of mesoporous ZnO nanosheets at room temperature. *Sens. Actuators B* **2019**, *293*, 83–92. [CrossRef]

42.   Law, J.B.K.; Thong, J.T.L. Simple fabrication of ZnO nanowire photodetector with fast photoresponse time. *Appl. Phys. Lett.* **2006**, *88*, 133114. [CrossRef]

43.   Chaaya, A.A.; Bechelany, M.; Balme, S.; Miele, P. ZnO 1D nanostructures designed by combining atomic layer deposition and electrospinning fo UV sensor applications. *J. Mater. Chem. A* **2014**, *2*, 20650. [CrossRef]

44.   Zhou, J.; Gu, Y.; Hu, Y.; Mai, W.; Yeh, P.H.; Bao, G.; Sood, A.K.; Polla, D.L.; Wang, Z.L. Gigantic enhancement in response and reset time of ZnO UV nanosensor by utilizing Schottky contact and surface functionalization. *Appl. Phys. Lett.* **2009**, *94*, 191103. [CrossRef] [PubMed]